
Kinematics of the Galaxy from Young Open Star Clusters with Data from the Gaia EDR3 Catalogue

V. V. Bobylev ¹ and A. T. Bajkova

*Pulkovo Astronomical Observatory, Russian Academy of Sciences,
Pulkovskoe sh. 65, St. Petersburg, 196140 Russia*

Abstract—We have analyzed the kinematics of open star clusters (OSCs) with the proper motions and distances calculated by Hao et al. based on Gaia EDR3 data. The mean line-of-sight velocities are known for a number of clusters from this list. We show that the Galactic rotation parameters determined from samples of OSCs with various ages are in good agreement between themselves. The most interesting results have been obtained from a sample of 967 youngest OSCs with a mean age of 18 Myr. In particular, we have found the following parameters of the angular velocity of Galactic rotation using only their proper motions and distances: $\Omega_0 = 28.01 \pm 0.15 \text{ km s}^{-1} \text{ kpc}^{-1}$, $\Omega'_0 = -3.674 \pm 0.040 \text{ km s}^{-1} \text{ kpc}^{-2}$, and $\Omega''_0 = 0.565 \pm 0.023 \text{ km s}^{-1} \text{ kpc}^{-3}$. The circular rotation velocity of the solar neighborhood around the Galactic center here is $V_0 = 226.9 \pm 3.1 \text{ km s}^{-1}$ for the adopted Galactocentric distance of the Sun $R_0 = 8.1 \pm 0.1 \text{ kpc}$. The parameters of the spiral density wave have been determined from the space velocities of 233 young clusters. The amplitudes of the radial and tangential velocity perturbations produced by the spiral density wave are $f_R = 9.1 \pm 0.8 \text{ km s}^{-1}$ and $f_\theta = 4.6 \pm 1.2 \text{ km s}^{-1}$, respectively; the perturbation wavelengths are $\lambda_R = 3.3 \pm 0.5 \text{ kpc}$ and $\lambda_\theta = 2.6 \pm 0.6 \text{ kpc}$ for the the adopted four-armed spiral pattern. The Sun's phase in the spiral density wave has been found to be $(\chi_\odot)_R \approx -180^\circ$.

INTRODUCTION

Open star clusters (OSCs) are of great importance for studying the structure and kinematics of the Galaxy. In particular, they are used to estimate the parameters of the Galactic rotation curve (Glushkova et al. 1998; Zabolotskikh et al. 2002; Loktin and Beshenov 2003; Piskunov et al. 2006; Loktin and Popova 2019), the geometrical and kinematic characteristics of the spiral density wave (Amaral and Lépine 1997; Popova and Loktin 2005; Loktin and Popova 2007; Naoz and Shaviv 2007; Bobylev et al. 2008; Lépine et al. 2008; Junqueira et al. 2015; Camargo et al. 2015; Bobylev and Bajkova 2019; Cantat-Gaudin et al. 2020), and their other structural and kinematic properties (Babusiaux et al. 2018; Kuhn et al. 2018; Tarricq et al. 2021; Monteiro et al. 2021).

The number of discovered and studied OSCs increases steadily (Dias et al. 2001, 2006, 2021; Kharchenko et al. 2005, 2007, 2013; Scholz et al. 2015; Cantat-Gaudin et al. 2018; Hao et al. 2021). The accuracy of their mean proper motions, line-of-sight velocities, and distances improves.

¹e-mail: vbobylev@gaoran.ru

The accuracy of the kinematic parameters of OSCs is of great importance for solving a great variety of kinematic problems. The distances to OSCs are commonly estimated with the help of the Hertzsprung–Russell diagram from photometric data or using other indirect methods (without trigonometric parallaxes). The implementation of the Gaia space experiment (Prusti et al. 2016) has made it possible not only to calculate highly accurate mean proper motions (Cantat-Gaudin et al. 2018) and line-of-sight velocities of OSCs, but also their mean trigonometric parallaxes (Cantat-Gaudin et al. 2020; Hao et al. 2021).

At present, the Gaia EDR3 (Gaia Early Data Release 3, Brown et al. 2021) version has been published, where, in comparison with the previous Gaia DR2 version (Brown et al. 2018), the trigonometric parallaxes and proper motions were improved approximately by 30% for ~ 1.5 billion stars. In the Gaia EDR3 catalogue the trigonometric parallaxes for ~ 500 million stars were measured with errors less than 0.2 milliarcseconds (mas), i.e., approximately a third of the stars with measured parallaxes. The proper motions for about a half of the stars in the catalogue were measured with a relative error less than 10%.

A slight systematic offset with respect to an inertial reference frame apparently remains in the Gaia EDR3 parallaxes (Ren et al. 2021; Maiz Apellániz 2021). This offset was first revealed in the Gaia DR2 parallaxes with $\Delta\pi = -0.029$ mas (Lindgren et al. 2018). This correction should be added to the measured parallaxes and, therefore, the true distances to stars must slightly decrease.

For stars with magnitudes $G < 15^m$ the random measurement errors of the proper motions lie within the range 0.02–0.04 mas yr $^{-1}$ (Brown et al. 2021), and they increase quite dramatically for fainter stars. There are no new line-of-sight velocity measurements in the Gaia EDR3 catalogue. Thus, the line-of-sight velocities for more than 7 million stars are taken from the Gaia DR2 version.

The goal of this paper is to determine the Galactic rotation parameters and spiral density wave parameters based on the latest data on OSCs. For this purpose, we use the mean proper motions and parallaxes of OSCs calculated by Hao et al. (2021) based on Gaia EDR3 data; the mean line-of-sight velocities are also available for a number of clusters.

METHOD

We have three stellar velocity components from observations: the line-of-sight velocity V_r and the two tangential velocity components $V_l = 4.74r\mu_l \cos b$ and $V_b = 4.74r\mu_b$, along the Galactic longitude l and latitude b respectively, expressed in km s $^{-1}$. Here, 4.74 is the dimension coefficient and r is the stellar heliocentric distance in kpc. The proper motion components $\mu_l \cos b$ and μ_b are expressed in mas yr $^{-1}$. The velocities U, V, W directed along the rectangular Galactic coordinate axes are calculated via the components V_r, V_l, V_b :

$$\begin{aligned} U &= V_r \cos l \cos b - V_l \sin l - V_b \cos l \sin b, \\ V &= V_r \sin l \cos b + V_l \cos l - V_b \sin l \sin b, \\ W &= V_r \sin b + V_b \cos b, \end{aligned} \tag{1}$$

where the velocity U is directed from the Sun toward the Galactic center, V is in the direction of Galactic rotation, and W is directed to the north Galactic pole. We can find two velocities, V_R directed radially away from the Galactic center and V_{circ} orthogonal to it pointing in the direction of Galactic rotation, based on the following relations:

$$\begin{aligned} V_{circ} &= U \sin \theta + (V_0 + V) \cos \theta, \\ V_R &= -U \cos \theta + (V_0 + V) \sin \theta, \end{aligned} \tag{2}$$

where the position angle θ obeys the relation $\tan \theta = y/(R_0 - x)$, x, y, z are the rectangular heliocentric coordinates of the star (the velocities U, V, W are directed along the corresponding x, y, z axes), and V_0 is the linear rotation velocity of the Galaxy at the solar distance R_0 . The velocities V_R and W are virtually independent of the pattern of the Galactic rotation curve. However, to analyze the periodicities in the tangential velocities, it is necessary to determine a smoothed Galactic rotation curve and to form the residual velocities ΔV_{circ} .

To determine the parameters of the Galactic rotation curve, we use the equations derived from Bottlinger's formulas, in which the angular velocity Ω is expanded into a series to terms of the second order of smallness in r/R_0 :

$$\begin{aligned} V_r = & -U_\odot \cos b \cos l - V_\odot \cos b \sin l - W_\odot \sin b \\ & + R_0(R - R_0) \sin l \cos b \Omega'_0 + 0.5R_0(R - R_0)^2 \sin l \cos b \Omega''_0, \end{aligned} \quad (3)$$

$$\begin{aligned} V_l = & U_\odot \sin l - V_\odot \cos l - r\Omega_0 \cos b \\ & + (R - R_0)(R_0 \cos l - r \cos b)\Omega'_0 + 0.5(R - R_0)^2(R_0 \cos l - r \cos b)\Omega''_0, \end{aligned} \quad (4)$$

$$\begin{aligned} V_b = & U_\odot \cos l \sin b + V_\odot \sin l \sin b - W_\odot \cos b \\ & - R_0(R - R_0) \sin l \sin b \Omega'_0 - 0.5R_0(R - R_0)^2 \sin l \sin b \Omega''_0, \end{aligned} \quad (5)$$

where R is the distance from the star to the Galactic rotation axis, $R^2 = r^2 \cos^2 b - 2R_0r \cos b \cos l + R_0^2$. The velocities $(U, V, W)_\odot$ are the mean group velocity of the sample, are taken with the opposite sign, and reflect the peculiar motion of the Sun; Ω_0 is the angular velocity of Galactic rotation at the solar distance R_0 , the parameters Ω'_0 and Ω''_0 are the corresponding derivatives of the angular velocity, and $V_0 = R_0|\Omega_0|$. The velocities V_R and ΔV_{circ} must be freed from the peculiar solar velocity $U_\odot, V_\odot, W_\odot$. In this paper R_0 is taken to be 8.1 ± 0.1 kpc, according to the review by Bobylev and Bajkova (2021), where it was derived as a weighted mean of a large number of present-day individual estimates.

The influence of the spiral density wave in the radial (V_R) and residual tangential (ΔV_{circ}) velocities is periodic with an amplitude $\sim 6 - 10$ km s $^{-1}$. According to the linear theory of density waves (Lin and Shu 1964), it is described by the following relations:

$$\begin{aligned} V_R = & -f_R \cos \chi, \\ \Delta V_{circ} = & f_\theta \sin \chi, \end{aligned} \quad (6)$$

where

$$\chi = m[\cot(i) \ln(R/R_0) - \theta] + \chi_\odot \quad (7)$$

is the phase of the spiral density wave (m is the number of spiral arms, i is the pitch angle of the spiral pattern, and χ_\odot is the Sun's radial phase in the spiral density wave); f_R and f_θ are the amplitudes of the radial and tangential velocity perturbations, which are assumed to be positive. The periodicities associated with the spiral density wave also manifest themselves in the vertical velocities W of young Galactic objects (Bobylev and Bajkova 2015; Rastorguev et al. 2017).

We apply a modified spectral analysis (Bajkova and Bobylev 2012) to study the periodicities in the velocities V_R and ΔV_{circ} . The wavelength λ (the distance between adjacent spiral arm segments measured along the radial direction) is calculated from the relation

$$2\pi R_0/\lambda = m \cot(|i|). \quad (8)$$

Let there be a series of measured velocities V_{R_n} (these can be both radial (V_R) and tangential (ΔV_{circ}) velocities), $n = 1, \dots, N$, where N is the number of objects. The objective of our

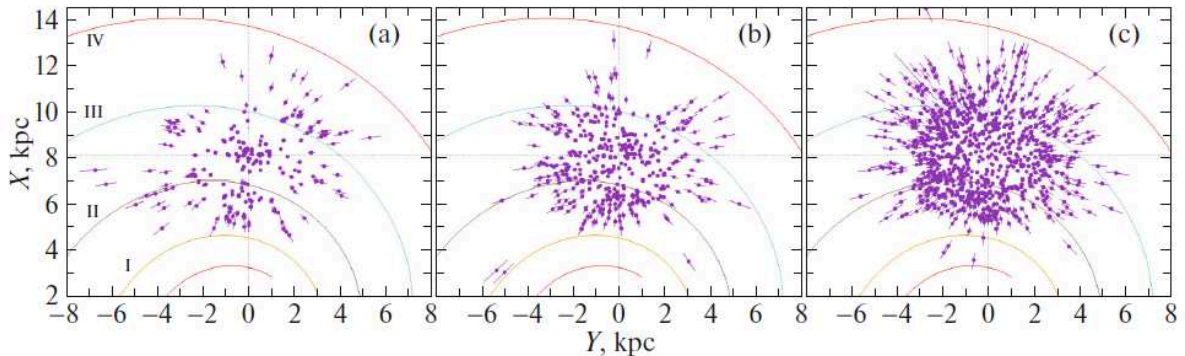


Figure 1: Distribution of OSCs younger than 60 Myr (a), with ages in the interval 60–300 Myr (b), and older than 300 Myr (c) on the Galactic XY plane; the four-armed spiral pattern with a pitch angle $i = -13^\circ$ (Bobylev and Bajkova 2014) is shown.

spectral analysis is to extract a periodicity from the data series in accordance with the adopted model describing a spiral density wave with parameters f , λ (or i) and χ_\odot .

Having taken into account the logarithmic behavior of the spiral density wave and the position angles of objects θ_n , our spectral (periodogram) analysis of the series of velocity perturbations is reduced to calculating the square of the amplitude (power spectrum) of the standard Fourier transform (Bajkova and Bobylev 2012):

$$\bar{V}_{\lambda_k} = \frac{1}{N} \sum_{n=1}^N V'_n(R'_n) \exp\left(-j \frac{2\pi R'_n}{\lambda_k}\right), \quad (9)$$

where \bar{V}_{λ_k} is the k th harmonic of the Fourier transform with wavelength $\lambda_k = D/k$, D is the period of the series being analyzed,

$$\begin{aligned} R'_n &= R_0 \ln(R_n/R_0), \\ V'_n(R'_n) &= V_n(R'_n) \times \exp(jm\theta_n). \end{aligned} \quad (10)$$

The sought-for wavelength λ corresponds to the peak value of the power spectrum S_{peak} . The pitch angle of the spiral density wave is found from Eq. (8). We determine the perturbation amplitude and phase by fitting the harmonic with the wavelength found to the observational data. The following relation can also be used to estimate the perturbation amplitude:

$$f_R(f_\theta) = 2 \times \sqrt{S_{peak}}. \quad (11)$$

DATA

Here the paper by Hao et al. (2021), where the mean proper motions and mean parallaxes of OSCs were calculated based on Gaia EDR3 data, served as the main data source. The age estimates were collected by these authors from various sources. The catalogue contains data on 3794 OSCs and, therefore, it is the most extensive kinematic database of Galactic OSCs to date.

The catalogue by Hao et al. (2021) provides the parallaxes π via which below we calculate the distances r from the formula $r = 1/\pi$. The relative errors of the mean OSC parallaxes

Table 1: The Galactic rotation parameters found from OSCs of various ages only from their proper motions (Eqs. (4) and (5)), N_* is the number of clusters used, \bar{t} is the mean age of the sample

Parameters	< 60 Myr	60 – 300 Myr	> 300 Myr
N_*	967	863	1794
\bar{t} , Myr	18	163	1100
\bar{z} , pc	-20 ± 4	-19 ± 8	-24 ± 9
U_\odot , km s $^{-1}$	7.34 ± 0.31	7.64 ± 0.44	8.64 ± 0.35
V_\odot , km s $^{-1}$	10.61 ± 0.45	13.07 ± 0.61	17.67 ± 0.46
W_\odot , km s $^{-1}$	7.45 ± 0.23	7.33 ± 0.31	6.55 ± 0.24
Ω_0 , km s $^{-1}$ kpc $^{-1}$	28.01 ± 0.15	26.96 ± 0.21	27.06 ± 0.16
Ω'_0 , km s $^{-1}$ kpc $^{-2}$	-3.674 ± 0.040	-3.629 ± 0.056	-3.284 ± 0.043
Ω''_0 , km s $^{-1}$ kpc $^{-3}$	0.565 ± 0.023	0.622 ± 0.034	0.463 ± 0.021
σ_0 , km s $^{-1}$	7.0	9.1	10.3
A , km s $^{-1}$ kpc $^{-1}$	14.88 ± 0.16	14.70 ± 0.23	13.30 ± 0.17
B , km s $^{-1}$ kpc $^{-1}$	-13.13 ± 0.22	-12.26 ± 0.31	-13.76 ± 0.24
V_0 , km s $^{-1}$	226.9 ± 3.1	218.4 ± 3.2	219.2 ± 3.0

in the entire catalogue are small, being, on average, $\sim 10\%$. There are isolated cases with parallax errors greater than 30%, and such OSCs are not used in this paper.

Figure 1 shows the distribution of OSCs from three samples of various ages in projection onto the Galactic XY plane. We use the coordinate system in which the X axis is directed from the Galactic center to the Sun and the direction of the Y axis coincides with the direction of Galactic rotation. The four-armed spiral pattern with a pitch angle $i = -13^\circ$ (Bobilev and Bajkova 2014) constructed with $R_0 = 8.1$ kpc is shown; the Roman numerals number the following spiral arm segments: Scutum (I), Carina-Sagittarius (II), Perseus (III), and the Outer Arm (IV).

The sample of OSCs younger than 60 Myr contains a total of 967 members with a mean age of 18 Myr. Figure 1a shows the distribution of 233 OSCs for which the line-of-sight velocities are available. Based on the space velocities of these clusters, we perform a spectral analysis to determine the parameters of the spiral density wave.

The sample of OSCs with ages in the interval 60–300 Myr contains a total of 863 members. Here, the mean age of the clusters is 163 Myr. Figure 1b shows the distribution of 398 OSCs for which the line-of-sight velocities are available.

The sample of OSCs older than 300 Myr contains a total of 1794 members. The mean age of the clusters in this sample is 1.1 Gyr. Figure 1c shows 1000 OSCs with the line-of-sight velocities.

Note that the distributions of all OSCs in projection onto the XY plane divided into four age intervals are shown in Fig. 1 from Hao et al. (2021). It can be clearly seen there that the OSCs younger than 20 Myr and those in the interval 20–200 Myr have a strong concentration toward the spiral arms.

Table 2: The Galactic rotation parameters found from OSCs of various ages through the simultaneous LSM solution of the system of three equations (3)–(5), N_\star is the number of clusters used, and NRV is the number of OSCs with the line-of-sight velocities

Parameters	< 60 Myr	60 – 300 Myr	> 300 Myr
N_\star	967	863	1794
N_{RV}	233	398	1000
U_\odot , km s ⁻¹	7.52 ± 0.33	8.57 ± 0.43	9.70 ± 0.38
V_\odot , km s ⁻¹	12.43 ± 0.45	13.58 ± 0.56	19.80 ± 0.46
W_\odot , km s ⁻¹	7.53 ± 0.27	7.37 ± 0.37	6.78 ± 0.33
Ω_0 , km s ⁻¹ kpc ⁻¹	28.07 ± 0.16	27.34 ± 0.22	27.62 ± 0.19
Ω'_0 , km s ⁻¹ kpc ⁻²	-3.713 ± 0.041	-3.782 ± 0.053	-3.486 ± 0.045
Ω''_0 , km s ⁻¹ kpc ⁻³	0.613 ± 0.025	0.674 ± 0.036	0.548 ± 0.024
σ_0 , km s ⁻¹	8.2	10.9	13.9
A , km s ⁻¹ kpc ⁻¹	15.04 ± 0.17	15.32 ± 0.21	14.12 ± 0.18
B , km s ⁻¹ kpc ⁻¹	-13.03 ± 0.23	-12.02 ± 0.31	-13.50 ± 0.26
V_0 , km s ⁻¹	227.3 ± 3.1	221.5 ± 3.3	223.7 ± 3.2

RESULTS

The system of conditional equations (3)–(5) is solved by the least-squares method (LSM) with weights of the form $w_r = S_0/\sqrt{S_0^2 + \sigma_{V_r}^2}$, $w_l = S_0/\sqrt{S_0^2 + \sigma_{V_l}^2}$ and $w_b = S_0/\sqrt{S_0^2 + \sigma_{V_b}^2}$, where S_0 is the “cosmic” dispersion, σ_{V_r} , σ_{V_l} , σ_{V_b} are the dispersions of the corresponding observed velocities. S_0 is comparable to the root-mean-square residual σ_0 (the error per unit weight) in solving the conditional equations (3)–(5). We adopted $S_0 = 7 - 8$ km s⁻¹ when analyzing the sample of young OSCs and $S_0 = 11 - 14$ km s⁻¹ for the sample of older OSCs. The system of equations (3)–(5) was solved in several iterations using the 3σ criterion to eliminate the OSCs with large residuals.

Method I

The first method consists in seeking a solution based only on the OSC proper motions. In this case, the system of two conditional equations (4) and (5) is solved.

The Galactic rotation parameters found for three samples of various ages are given in Table 1. For each sample we calculated the mean age t and the mean coordinate z (reflects the Sun’s elevation above the Galactic plane). Note that the values of z found are in excellent agreement with $z = -23 \pm 3$ pc found by analyzing OSCs with data from the Gaia DR2 catalogue in Cantat-Gaudin et al. (2020).

The Oort constants $A = 0.5\Omega'_0 R_0$ and $B = A - \Omega_0$ calculated using the deduced Ω_0 and Ω'_0 are given in the lower part of the table. The linear Galactic rotation velocity at the solar distance $V_0 = R_0|\Omega_0|$ for the adopted $R_0 = 8.1 \pm 0.1$ kpc is also given.

Based on the entire sample of 3624 OSCs, we found the velocity components $(U, V, W)_\odot = (7.89, 14.35, 6.97) \pm (0.22, 0.29, 0.16)$ km s⁻¹ and the following parameters of the angular

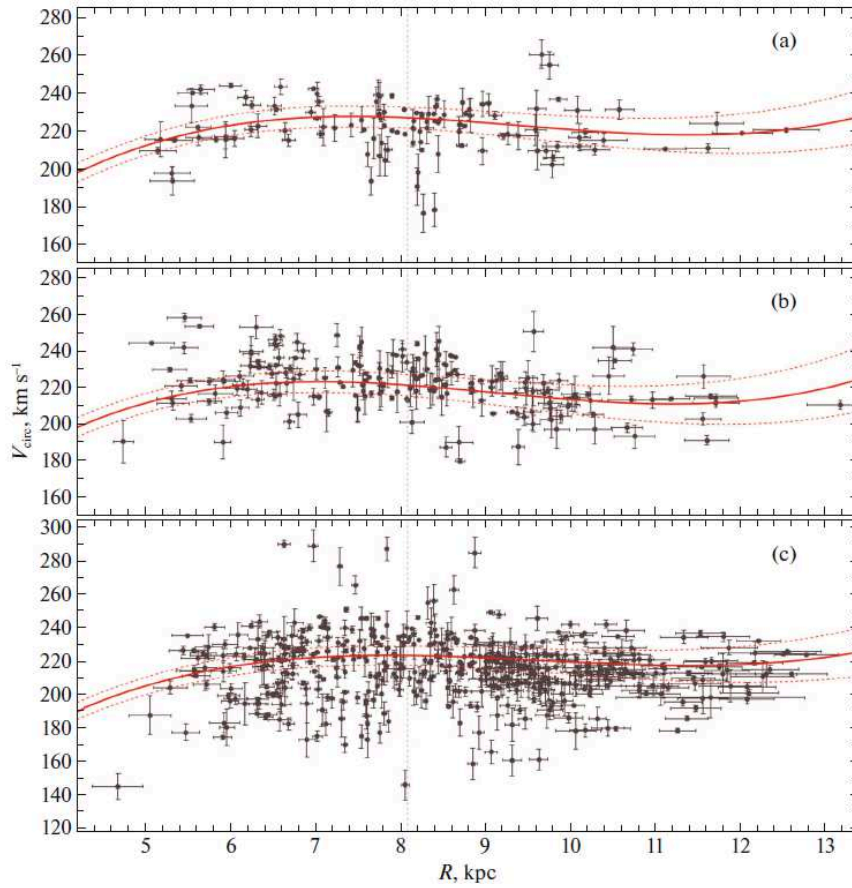


Figure 2: Circular rotation velocities V_{circ} versus distance R for the youngest OSCs (a), with ages in the interval 60–300 Myr (b), and older than 300 Myr (c); the Galactic rotation curve found from these OSCs with an indication of the boundaries of the 1σ confidence regions is shown for each sample.

velocity of Galactic rotation by this method:

$$\begin{aligned}
 \Omega_0 &= 27.37 \pm 0.10 \text{ km s}^{-1} \text{ kpc}^{-1}, \\
 \Omega'_0 &= -3.510 \pm 0.027 \text{ km s}^{-1} \text{ kpc}^{-2}, \\
 \Omega''_0 &= 0.534 \pm 0.014 \text{ km s}^{-1} \text{ kpc}^{-3}.
 \end{aligned}
 \tag{12}$$

In this solution the error per unit weight is $\sigma_0 = 9.4 \text{ km s}^{-1}$. The linear Galactic rotation velocity at the solar distance is $V_0 = 221.7 \pm 2.9 \text{ km s}^{-1}$, while the Oort constants are $A = 14.21 \pm 0.11 \text{ km s}^{-1} \text{ kpc}^{-1}$ and $B = -13.15 \pm 0.15 \text{ km s}^{-1} \text{ kpc}^{-1}$.

Method II

In this approach we use all of the available data. The clusters with the proper motions, line-of-sight velocities, and distances give all three equations (3)–(5), while the clusters for which only the proper motions are available give only two equations, (4) and (5). We solve this system of equations simultaneously.

The Galactic rotation parameters found by this method for three samples of OSCs with various ages are presented in Table 2. The number of OSCs with the line-of-sight velocities

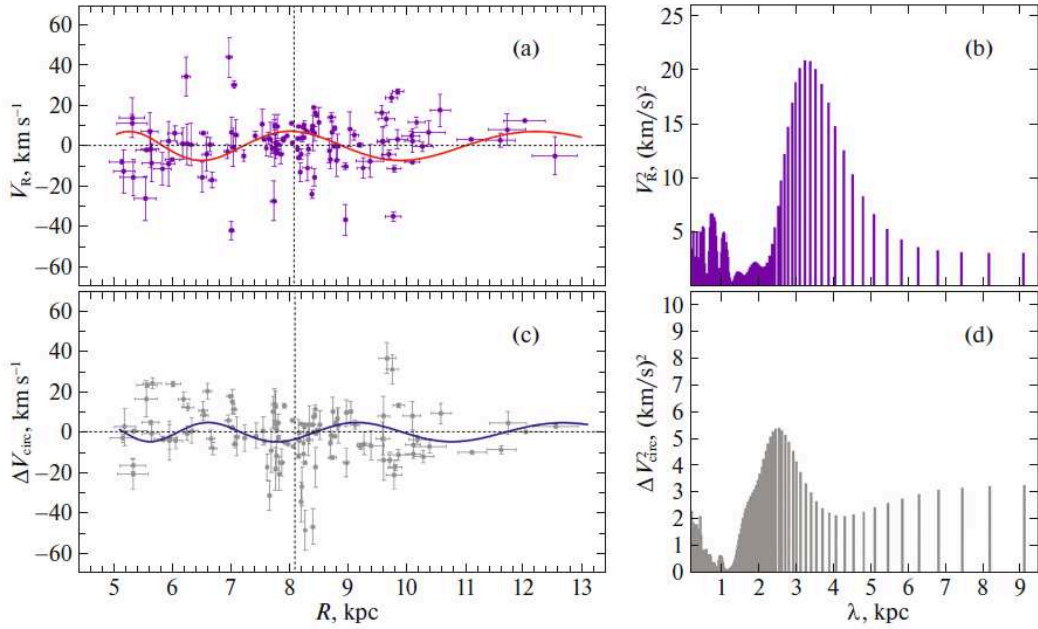


Figure 3: Radial velocities V_R versus distance R for the youngest OSCs (a), the power spectrum of this sample (b), the residual rotation velocities ΔV_{circ} of the youngest OSCs (c), and their power spectrum (d).

N_{RV} used in the solution is given. At the same time, the OSCs with errors in their mean line-of-sight velocities greater than 10 km s^{-1} were not used.

As a result of using the data on all 3624 OSCs, we found $(U, V, W)_{\odot} = (8.73, 16.03, 7.10) \pm (0.24, 0.30, 0.20) \text{ km s}^{-1}$ and

$$\begin{aligned}
 \Omega_0 &= 27.79 \pm 0.12 \text{ km s}^{-1} \text{ kpc}^{-1}, \\
 \Omega'_0 &= -3.669 \pm 0.028 \text{ km s}^{-1} \text{ kpc}^{-2}, \\
 \Omega''_0 &= 0.606 \pm 0.016 \text{ km s}^{-1} \text{ kpc}^{-3}.
 \end{aligned}
 \tag{13}$$

In this solution the error per unit weight is $\sigma_0 = 12.0 \text{ km s}^{-1}$. The linear Galactic rotation velocity at the solar distance is $V_0 = 225.1 \pm 2.9 \text{ km s}^{-1}$, while the Oort constants are $A = 14.86 \pm 0.11 \text{ km s}^{-1} \text{ kpc}^{-1}$ and $B = -12.93 \pm 0.16 \text{ km s}^{-1} \text{ kpc}^{-1}$.

As can be seen from a comparison of the parameters (12) and (13) as well as Tables 1 and 2, invoking the line-of-sight velocities leads to an increase in the dispersion of the estimates.

In Fig. 2 the circular rotation velocities V_{circ} are plotted against the distance R for three samples of OSCs with various ages. The parameters from the corresponding column in Table 2 were taken to construct the rotation curve for each sample. We see good agreement between these Galactic rotation curves. Therefore, any of them can be used to form the residual velocities ΔV_{circ} for a further spectral analysis.

Note that we deem the Galactic rotation curve obtained with the smallest error per unit weight $\sigma_0 = 7 \text{ km s}^{-1}$ to be the best one. The parameters of this rotation curve found by method I only from the proper motions of the youngest OSCs are given in the first column of Table 1.

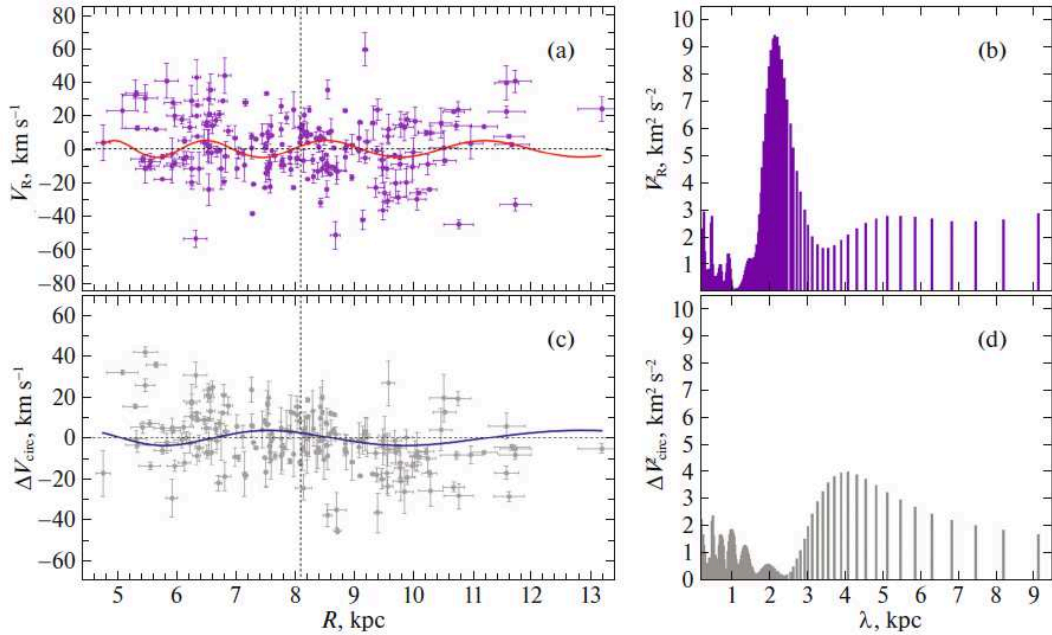


Figure 4: Radial velocities V_R versus distance R for OSCs with ages in the interval 60–300 Myr (a), the power spectrum of this sample (b), the residual rotation velocities ΔV_{circ} for OSCs with ages in the interval 60–300 Myr (c), and their power spectrum (d).

Spectral Analysis

First we determined the parameters of the spiral density wave based on the sample of youngest OSCs with ages less than 60 Myr (with a mean age of 18 Myr). For this purpose, we used 233 OSCs for which the line-of-sight velocities are available. A spectral analysis of their radial and residual tangential velocities showed that the perturbation wavelengths and velocity perturbations found independently for each type of velocities agree in principle.

The results of our spectral analysis of the OSCs from this sample are presented in Fig. 3. The figure shows the radial velocities V_R and residual rotation velocities ΔV_{circ} as a function of distance R and their power spectra.

Based on 233 OSCs from this sample, we found the wavelengths $\lambda_R = 3.3 \pm 0.5$ kpc and $\lambda_\theta = 2.6 \pm 0.6$ kpc. For the four-armed spiral pattern ($m = 4$ and the adopted R_0) the pitch angles $i_R = -14.5 \pm 2.1^\circ$ and $i_\theta = -11.4 \pm 2.6^\circ$ correspond to these values. The Sun’s phase in the spiral density wave is $(\chi_\odot)_R \approx -180^\circ$ and $(\chi_\odot)_\theta \approx -120^\circ$; we measure it from the presumed center of the Carina–Sagittarius arm—from $R \sim 7$ kpc in the direction of increasing R . The amplitudes of the radial and tangential velocity perturbations are $f_R = 9.1 \pm 0.8$ km s⁻¹ and $f_\theta = 4.6 \pm 1.2$ km s⁻¹, respectively.

A spectral analysis of the space velocities of OSCs with ages in the interval 60–300 Myr showed that there is also an influence of the spiral density wave in them. The results of our spectral analysis of the OSCs from this sample are presented in Fig. 4, where the velocities V_R and ΔV_{circ} and their power spectra are shown.

Based on 398 OSCs from this sample, we found the perturbation wavelengths $\lambda_R = 2.2 \pm 0.6$ kpc and $\lambda_\theta = 4.1 \pm 0.8$ kpc. For the four-armed spiral pattern ($m = 4$ and the adopted R_0) the pitch angles $i_R = -9.6 \pm 2.6^\circ$ and $i_\theta = -17.9 \pm 3.3^\circ$ correspond

to these values. The amplitudes of the radial and tangential velocity perturbations are $f_R = 6.1 \pm 1.8 \text{ km s}^{-1}$ and $f_\theta = 3.9 \pm 2.2 \text{ km s}^{-1}$, respectively. The Sun's phase in the spiral density wave χ_\odot here is $(\chi_\odot)_R \approx -90^\circ$ and $(\chi_\odot)_\theta \approx -180^\circ$. We see that the parameters of the spiral density wave are determined from the radial velocities of these OSCs quite reliably and in agreement with the results described above.

DISCUSSION

Velocities $(U, V, W)_\odot$

The velocities $(U, V, W)_\odot$ are the group velocity of the OSC sample under consideration taken with the opposite sign. These velocities contain the peculiar motion of the Sun relative to the local standard of rest, the perturbations from the spiral density wave (for relatively young objects), and the influence of the so-called asymmetric drift (lagging behind the circular rotation velocity with sample age) on the velocity V_\odot .

The components of the peculiar solar velocity relative to the local standard of rest are currently believed to have been determined most reliably in Schönrich et al. (2010), $(U, V, W)_\odot = (11.1, 12.2, 7.3) \pm (0.7, 0.5, 0.4) \text{ km s}^{-1}$. We can see that the velocities U_\odot and W_\odot found in this paper from various OSC samples agree, within the error limits, with the estimates by Schönrich et al. (2010). In addition, an increase in the velocity V_\odot with OSC age can be seen in our results, which is a manifestation of the asymmetric drift.

Galactic Rotation

The most important local parameter is the linear velocity V_0 . Such objects of the Galactic thin disk as hydrogen clouds, maser sources, O- and B-type stars, young OSCs, Cepheids, etc. possess the most rapid rotation.

For example, Bobylev et al. (2016) obtained an estimate of $V_0 = 236 \pm 6 \text{ km s}^{-1}$ for the adopted $R_0 = 8.3 \pm 0.2 \text{ kpc}$ by analyzing a sample of OSCs younger than 50 Myr from the Milky Way Star Clusters (MWSC) catalogue (Kharchenko et al. 2013). While analyzing about 770 Cepheids with known line-of-sight velocities, Mróz et al. (2019) obtained an estimate of $V_0 = 233.6 \pm 2.8 \text{ km s}^{-1}$ for the adopted $R_0 = 8.122 \pm 0.031 \text{ kpc}$. Using about 3500 classical Cepheids, Ablimit et al. (2020) constructed the Galactic rotation curve in the range of distances R : 4–19 kpc and found the velocity $V_0 = 232.5 \pm 0.9 \text{ km s}^{-1}$ for the adopted $R_0 = 8.122 \pm 0.031 \text{ kpc}$ with a very high accuracy. Having analyzed 800 Cepheids with known line-of-sight velocities, Bobylev et al. (2021) found $V_0 = 240 \pm 3 \text{ km s}^{-1}$ for the inferred $R_0 = 8.27 \pm 0.10 \text{ kpc}$.

Note several determinations of the parameters of the angular velocity of Galactic rotation using various data. For example, based on 130 Galactic masers with measured trigonometric parallaxes, Rastorguev et al. (2017) obtained the following estimates: $(U, V)_\odot = (11.40, 17.23) \pm (1.33, 1.09) \text{ km s}^{-1}$, $\Omega_0 = 28.93 \pm 0.53 \text{ km s}^{-1} \text{ kpc}^{-1}$, $\Omega'_0 = -3.96 \pm 0.07 \text{ km s}^{-1} \text{ kpc}^{-2}$ and $\Omega''_0 = 0.87 \pm 0.03 \text{ km s}^{-1} \text{ kpc}^{-3}$, where the linear velocity V_0 is $243 \pm 10 \text{ km s}^{-1}$ for $R_0 = 8.40 \pm 0.12 \text{ kpc}$ found.

Based on a sample of 495 OB stars with their proper motions from the Gaia DR2 catalogue (Brown et al. 2018), Bobylev and Bajkova (2018) found the following parameters: $(U, V, W)_\odot = (8.16, 11.19, 8.55) \pm (0.48, 0.56, 0.48) \text{ km s}^{-1}$, $\Omega_0 = 28.92 \pm 0.39 \text{ km s}^{-1}$

kpc^{-1} , $\Omega'_0 = -4.087 \pm 0.083 \text{ km s}^{-1} \text{ kpc}^{-2}$ and $\Omega''_0 = 0.703 \pm 0.067 \text{ km s}^{-1} \text{ kpc}^{-3}$, where $V_0 = 231 \pm 5 \text{ km s}^{-1}$ for adopted $R_0 = 8.0 \pm 0.15 \text{ kpc}$.

Based on a sample of 788 Cepheids from the list of Mróz et al. (2019) with their proper motions and line-of-sight velocities from the Gaia DR2 catalogue, Bobylev et al. (2021) found $(U_\odot, V_\odot, W_\odot) = (10.1, 13.6, 7.0) \pm (0.5, 0.6, 0.4) \text{ km s}^{-1}$, and: $\Omega_0 = 29.05 \pm 0.15 \text{ km s}^{-1} \text{ kpc}^{-1}$, $\Omega'_0 = -3.789 \pm 0.045 \text{ km s}^{-1} \text{ kpc}^{-2}$, $\Omega''_0 = 0.722 \pm 0.027 \text{ km s}^{-1} \text{ kpc}^{-3}$, $\Omega'''_0 = -0.087 \pm 0.007 \text{ km s}^{-1} \text{ kpc}^{-4}$, $R_0 = 8.27 \pm 0.10 \text{ kpc}$.

Based on a sample of 147 masers, Reid et al. (2019) found the following values of the two most important kinematic parameters: $R_0 = 8.15 \pm 0.15 \text{ kpc}$ and $\Omega_\odot = 30.32 \pm 0.27 \text{ km s}^{-1} \text{ kpc}^{-1}$, where $\Omega_\odot = \Omega_0 + V_\odot/R$. The velocity $V_\odot = 12.24 \text{ km s}^{-1}$ was taken from Schönrich et al. (2010). These authors used an expansion of the linear Galactic rotation velocity into a series.

The Oort constants A and B are also of interest. For example, having analyzed the proper motions and parallaxes of a local sample of 304 267 main-sequence stars from the Gaia DR1 catalogue (Brown et al. 2016), Bovy (2017) found $A = 15.3 \pm 0.5 \text{ km s}^{-1} \text{ kpc}^{-1}$ and $B = -11.9 \pm 0.4 \text{ km s}^{-1} \text{ kpc}^{-1}$, based on which he estimated the angular velocity of Galactic rotation $\Omega_0 = 27.1 \pm 0.5 \text{ km s}^{-1} \text{ kpc}^{-1}$ and the velocity $V_0 = 219 \pm 4 \text{ km s}^{-1}$. Based on a sample of 5627 A-type stars close ($r < 0.6 \text{ kpc}$) to the Sun from the LAMOST DR4 (The Large Sky Area Multi-Object Fiber Spectroscopic Telescope) catalogue (Cui et al. 2012; Xiang et al. 2017), Wang et al. (2021) obtained the following estimates of the Oort constants: $A = 16.31 \pm 0.89 \text{ km s}^{-1} \text{ kpc}^{-1}$ and $B = -11.99 \pm 0.79 \text{ km s}^{-1} \text{ kpc}^{-1}$, where $\Omega_0 = 28.30 \pm 1.19 \text{ km s}^{-1} \text{ kpc}^{-1}$.

It can be concluded that the velocity V_0 found in this paper from the youngest OSCs is in excellent agreement with the estimates of this velocity obtained from other young objects of the Galactic disk. The parameters Ω_0 , Ω'_0 and Ω''_0 , as well as the Oort constants A and B were determined in this paper with a high accuracy; their values are also in good agreement with the estimates of other authors.

Spiral Density Wave Parameters

Mel'nik et al. (2001) found $f_R = 7 \pm 1 \text{ km s}^{-1}$, $f_\theta = 2 \pm 1 \text{ km s}^{-1}$, and $\lambda = 2.0 \pm 0.2 \text{ kpc}$ for $m = 2$ by analyzing OB associations. Zabolotskikh et al. (2002) found $f_R = 7 \pm 2 \text{ km s}^{-1}$, $f_\theta = 1 \pm 2 \text{ km s}^{-1}$, and $i = -6.0 \pm 0.9^\circ$ for $m = 2$ with a phase $\chi_\odot \approx -85^\circ$ based on young Cepheids ($P > 9^d$) and OSCs ($\log t < 7.6$); $f_R = 6.6 \pm 2.5 \text{ km s}^{-1}$, $f_\theta = 0.4 \pm 2 \text{ km s}^{-1}$, and $i = -6.6 \pm 0.9^\circ$ for $m = 2$ with a phase $\chi_\odot \approx -97^\circ$ based on OB stars.

Having analyzed the spatial distribution of a large sample of classical Cepheids, Dambis et al. (2015) estimated the pitch angle of the spiral pattern $i = -9.5 \pm 0.1^\circ$ and the Sun's phase $\chi_\odot = -121 \pm 3^\circ$ for the four-armed spiral pattern.

Based on a sample of OSCs younger than 50 Myr from the MWSC catalogue (Kharchenko et al. 2013), Bobylev et al. (2016) found $f_\theta = 5.6 \pm 1.6 \text{ km s}^{-1}$ and $f_R = 7.7 \pm 1.4 \text{ km s}^{-1}$, the perturbation wavelengths $\lambda_\theta = 2.6 \pm 0.5 \text{ kpc}$ ($i_\theta = -11 \pm 2^\circ$) and $\lambda_R = 2.1 \pm 0.5 \text{ kpc}$ ($i_R = -9 \pm 2^\circ$) for the adopted four-armed spiral pattern ($m = 4$).

Having analyzed maser sources with VLBI parallaxes, Rastorguev et al. (2017) found $i = -10.4 \pm 0.3^\circ$ and $\chi_\odot = -125 \pm 10^\circ$, in good agreement with our results.

Loktin and Popova (2019) found $f_R = 4.6 \pm 0.7 \text{ km s}^{-1}$ and $f_\theta = 1.1 \pm 0.4 \text{ km s}^{-1}$ based on OSCs from the Homogenous Catalogue of Open Cluster Parameters with their proper motions from the Gaia DR2 catalogue. A review of the determinations of the velocity

perturbations f_R and f_θ made in recent years by various authors using various spiral structure indicators can be found in the paper of these authors.

While analyzing 326 young ($\log t < 8$) OSCs with the proper motions and distances calculated from Gaia DR2 data, Bobilev and Bajkova (2019) obtained the following estimates: $f_\theta = 3.8 \pm 1.2 \text{ km s}^{-1}$ and $f_R = 4.7 \pm 1.0 \text{ km s}^{-1}$, $\lambda_\theta = 2.3 \pm 0.5 \text{ kpc}$ and $\lambda_R = 2.2 \pm 0.5 \text{ kpc}$ ($m = 4$, $R_0 = 8.0 \pm 0.15 \text{ kpc}$), and $\chi_\odot = -120^\circ \pm 10^\circ$.

It can be noted that the amplitude of the tangential perturbations f_θ is usually determined poorly. As simulations of density waves in the Galaxy showed (Burton 1971), the expected perturbation amplitudes at the solar distance can reach $f_R \sim 8 \text{ km s}^{-1}$ and $f_\theta \sim 6 \text{ km s}^{-1}$. We see that $f_R = 9.1 \pm 0.8 \text{ km s}^{-1}$ found in this paper from the youngest OSCs is in excellent agreement with the expected estimate.

Based on OSCs with a mean age of 163 Myr, the parameters of the spiral density wave are well determined from the radial velocities. The Sun's phases $(\chi_\odot)_R$ are of greatest interest here: -180° and -90° for OSCs with a mean age of 18 and 163 Myr, respectively, which show that the wave moves.

CONCLUSIONS

We studied a sample of OSCs with their proper motions and parallaxes from the Gaia EDR3 catalogue. The catalogue by Hao et al. (2021), which contains data on 3794 OSCs with various ages, served for this purpose. The mean line-of-sight velocities are known approximately for a third of the clusters from this catalogue.

We showed that the Galactic rotation parameters determined from samples of OSCs with various ages are in good agreement between themselves; the methods of analysis using the space velocities and only the proper motions of OSCs were applied. In particular, the linear rotation velocity of the solar neighborhood V_0 varies from $218 \pm 3 \text{ km s}^{-1}$ found from relatively old OSCs to $227 \pm 3 \text{ km s}^{-1}$ typical for the youngest OSCs.

We analyzed in detail the kinematics of 967 youngest OSCs with a mean age of 18 Myr. Primarily these OSCs were used to redetermine the Galactic rotation parameters. Using only their proper motions and parallaxes, based on a nonlinear rotation model, we found the following parameters of the angular velocity of Galactic rotation: $\Omega_0 = 28.01 \pm 0.15 \text{ km s}^{-1} \text{ kpc}^{-1}$, $\Omega'_0 = -3.674 \pm 0.040 \text{ km s}^{-1} \text{ kpc}^{-2}$ and $\Omega''_0 = 0.565 \pm 0.023 \text{ km s}^{-1} \text{ kpc}^{-3}$. Here, the circular rotation velocity of the solar neighborhood around the Galactic center is $V_0 = 226.9 \pm 3.1 \text{ km s}^{-1}$ for the adopted distance $R_0 = 8.1 \pm 0.1 \text{ kpc}$.

To determine the parameters of the spiral density wave, we applied a method based on a periodogram Fourier analysis. This method takes into account both the logarithmic behavior of the Galactic spiral pattern and the position angles of objects, which makes it possible to perform an accurate analysis of the velocities of objects distributed in a wide range of Galactocentric distances.

Initially, such an analysis was applied to the sample of 233 youngest OSCs with measured line-of-sight velocities. We showed that the perturbation wavelengths and velocity perturbations found independently for each type of velocities, $\lambda_R = 3.3 \pm 0.5 \text{ kpc}$ and $\lambda_\theta = 2.6 \pm 0.6 \text{ kpc}$, agree in principle. For the four-armed spiral pattern ($m = 4$ and the adopted R_0) the pitch angles $i_R = -14.5 \pm 2.1^\circ$ and $i_\theta = -11.4 \pm 2.6^\circ$ correspond to these values. The Sun's phase in the spiral density wave is $(\chi_\odot)_R \approx -180^\circ$ and $(\chi_\odot)_\theta \approx -120^\circ$. The amplitudes of the radial and tangential velocity perturbations are $f_R = 9.1 \pm 0.8 \text{ km}$

s^{-1} and $f_\theta = 4.6 \pm 1.2 \text{ km s}^{-1}$, respectively.

Then, we showed that the influence of the spiral density wave also manifests itself in the space velocities of OSCs with ages in the interval 60–300 Myr (a mean age of 163 Myr). Based on 398 OSCs from this sample, we performed a spectral analysis of their radial and residual tangential velocities. The parameters of the spiral density wave are well determined from the radial velocities of these OSCs. For example, the perturbation wavelength and velocity perturbations were found to be $\lambda_R = 2.2 \pm 0.6 \text{ kpc}$ ($i_R = -9.6 \pm 2.6^\circ$ for $m = 4$ and the adopted R_0), $f_R = 6.1 \pm 1.8 \text{ km s}^{-1}$ and $f_\theta = 3.9 \pm 2.2 \text{ km s}^{-1}$. The Sun's phase in the spiral density wave here is $(\chi_\odot)_R \approx -90^\circ$ and $(\chi_\odot)_\theta \approx -180^\circ$.

REFERENCES

1. I. Ablimit, G. Zhao, C. Flynn, and S. A. Bird, *Astrophys. J.* 895, L12 (2020).
2. L. H. Amaral and J. R. D. Lépine, *Mon. Not. R. Astron. Soc.* 286, 885 (1997).
3. C. Babusiaux, F. van Leeuwen, M. A. Barstow, et al. (Gaia Collab.), *Astron. Astrophys.* 616, 10 (2018).
4. A. T. Bajkova and V. V. Bobylev, *Astron. Lett.* 38, 549 (2012).
5. V. V. Bobylev, A. T. Bajkova, and A. S. Stepanishchev, *Astron. Lett.* 34, 515 (2008).
6. V. V. Bobylev and A. T. Bajkova, *Mon. Not. R. Astron. Soc.* 437, 1549 (2014).
7. V. V. Bobylev and A. T. Bajkova, *Mon. Not. R. Astron. Soc.* 447, L50 (2015).
8. V. V. Bobylev, A. T. Bajkova, and K. S. Shirokova, *Astron. Lett.* 42, 721 (2016).
9. V. V. Bobylev and A. T. Bajkova, *Astron. Lett.* 44, 675 (2018).
10. V. V. Bobylev and A. T. Bajkova, *Astron. Lett.* 45, 109 (2019).
11. V. V. Bobylev and A. T. Bajkova, *Astron. Rep.* 65, 498 (2021).
12. V. V. Bobylev, A. T. Bajkova, A. S. Rastorguev, and M. V. Zabolotskikh, *Mon. Not. R. Astron. Soc.* 502, 4377 (2021).
13. J. Bovy, *Mon. Not. R. Astron. Soc.* 468, L63 (2017).
14. A. G. A. Brown, A. Vallenari, T. Prusti, et al. (Gaia Collab.), *Astron. Astrophys.* 595, 2 (2016).
15. A. G. A. Brown, A. Vallenari, T. Prusti, et al. (Gaia Collab.), *Astron. Astrophys.* 616, 1 (2018).
16. A. G. A. Brown, A. Vallenari, T. Prusti, et al. (Gaia Collab.), *Astron. Astrophys.* 649, 1 (2021).
17. W. B. Burton, *Astron. Astrophys.* 10, 76 (1971).
18. D. Camargo, C. Bonatto, and E. Bica, *Mon. Not. R. Astron. Soc.* 450, 4150 (2015).
19. T. Cantat-Gaudin, C. Jordi, A. Vallenari, et al., *Astron. Astrophys.* 618, A93 (2018).
20. T. Cantat-Gaudin, F. Anders, A. Castro-Ginard, et al., *Astron. Astrophys.* 640, A1 (2020).
21. X.-Q. Cui, Y.-H. Zhao, Y.-Q. Chu, et al., *Res. Astron. Astrophys.* 12, 1197 (2012).
22. A. K. Dambis, L. N. Berdnikov, Yu. N. Efremov, et al., *Astron. Lett.* 41, 489 (2015).
23. W. S. Dias, J. R. D. Lépine, and B. S. Alessi, *Astron. Astrophys.* 376, 441 (2001).
24. W. S. Dias, M. Assafin, V. Flório, B. S. Alessi, and V. Libero, *Astron. Astrophys.* 446, 949 (2006).
25. W. S. Dias, H. Monteiro, A. Moitinho, et al., *Mon. Not. R. Astron. Soc.* 504, 356 (2021).
26. E. V. Glushkova, A. K. Dambis, A. M. Mel'nik, and A. S. Rastorguev, *Astron. Astrophys.* 329, 514 (1998).
27. C. J. Hao, Y. Xu, L. G. Hou, et al., *Astron. Astrophys.* 652, 102 (2021).
28. T. C. Junqueira, C. Chiappini, J. R. D. Lépine, I. Minchev, and B. X. Santiago, *Mon. Not. R. Astron. Soc.* 449, 2336 (2015).

29. N. V. Kharchenko, A. E. Piskunov, S. Röser, E. Schilbach, and R.-D. Scholz, *Astron. Astrophys.* 438, 1163 (2005).
30. N. V. Kharchenko, R.-D. Scholz, A. E. Piskunov, S. Röser, and E. Schilbach, *Astron. Nachr.* 328, 889 (2007).
31. N. V. Kharchenko, A. E. Piskunov, E. Schilbach, S. Röser, and R.-D. Scholz, *Astron. Astrophys.* 558, A53 (2013).
32. M. A. Kuhn, L. A. Hillenbrand, A. Sills, E. D. Feigelson, and K. V. Getman, *Astron. Astrophys. J.* 870, 32 (2018).
33. J. R. D. Lépine, W. S. Dias, and Yu. Mishurov, *Mon. Not. R. Astron. Soc.* 386, 2081 (2008).
34. C. C. Lin and F. H. Shu, *Astron. Astrophys. J.* 140, 646 (1964).
35. L. Lindgren, J. Hernandez, A. Bombrun, et al. (Gaia Collab.), *Astron. Astrophys.* 616, 2 (2018).
36. A. V. Loktin and G. V. Beshenov, *Astron. Rep.* 47, 6 (2003).
37. A. V. Loktin and M. E. Popova, *Astron. Rep.* 51, 364 (2007).
38. A. V. Loktin and M. E. Popova, *Astron. Rep.* 74, 270 (2019).
39. J. Maiz Apellániz, arXiv: 2110.01475 (2021).
40. A. M. Mel'nik, A. K. Dambis, and A. S. Rastorguev, *Astron. Lett.* 27, 611 (2001).
41. H. Monteiro, D. A. Barros, W. S. Dias, and J. R. D. Lépine, *Front. Astron. Space Sci.* 8, 62 (2021).
42. P. Mróz, A. Udalski, D. M. Skowron, et al., *Astron. Astrophys. J.* 870, L10 (2019).
43. S. Naoz and N. J. Shaviv, *New Astron.* 12, 410 (2007).
44. A. E. Piskunov, N. V. Kharchenko, S. Röser, E. Schilbach, and R.-D. Scholz, *Astron. Astrophys.* 445, 545 (2006).
45. M. E. Popova and A. V. Loktin, *Astron. Lett.* 31, 171 (2005).
46. T. Prusti, J. H. J. de Bruijne, A. G. A. Brown, et al. (Gaia Collab.), *Astron. Astrophys.* 595, 1 (2016).
47. A. S. Rastorguev, M. V. Zabolotskikh, A. K. Dambis, N. D. Utkin, V. V. Bobylev, and A. T. Bajkova, *Astron. Astrophys. Bull.* 72, 122 (2017).
48. M. J. Reid, K. M. Menten, A. Brunthaler, et al., *Astron. Astrophys. J.* 885, 131 (2019).
49. F. Ren, X. Chen, H. Zhang, R. de Grijs, L. Deng, and Yang Huang, *Astron. Astrophys. J. Lett.* 911, 20 (2021).
50. R.-D. Scholz, N. V. Kharchenko, A. E. Piskunov, S. Röser, and E. Schilbach, *Astron. Astrophys.* 581, A39 (2015).
51. R. Schönrich, J. J. Binney, and W. Dehnen, *Mon. Not. R. Astron. Soc.* 403, 1829 (2010).
52. Y. Tarricq, C. Soubiran, L. Casamiquela, et al., *Astron. Astrophys.* 647, A19 (2021).
53. F. Wang, H.-W. Zhang, Y. Huang, et al., *Mon. Not. R. Astron. Soc.* 504, 199 (2021).
54. M.-S. Xiang, X.-W. Liu, H.-B. Yuan, et al., *Mon. Not. R. Astron. Soc.* 467, 1890 (2017).
55. M. V. Zabolotskikh, A. S. Rastorguev, and A. K. Dambis, *Astron. Lett.* 28, 454 (2002).